Lattice Dynamics Study of HgGa2Se4 at High Pressures

11 AUTHORS, INCLUDING:

Oscar Gomis
Universitat Politècnica de València
85 PUBLICATIONS **760** CITATIONS

SEE PROFILE

Francisco Javier Manjon
Universitat Politècnica de València
148 PUBLICATIONS **2,480** CITATIONS

SEE PROFILE

Placida Rodriguez
Universidad de La Laguna
108 PUBLICATIONS **1,847** CITATIONS

SEE PROFILE

Ion Tiginyanu
Academy of Sciences of Moldova
390 PUBLICATIONS **3,817** CITATIONS

SEE PROFILE

Lattice Dynamics Study of HgGa₂Se₄ at High Pressures

R. Vilaplana,*,[†] O. Gomis,[†] F. J. Manjón,[‡] H. M. Ortiz,[‡,§,○] E. Pérez-González,[∥] J. López-Solano,[∥]
P. Rodríguez-Hernández,[∥] A. Muñoz,[∥] D. Errandonea,[⊥] V. V. Ursaki,[#] and I. M. Tiginyanu[#]

[†]Centro de Tecnologías Físicas: Acústica, Materiales y Astrofísica, MALTA Consolider Team, Universitat Politècnica de València, 46022 València, Spain

[‡]Instituto de Diseño para la Fabricación y Producción Automatizada, MALTA Consolider Team, Universitat Politècnica de València, 46022 València, Spain

[§]CINVESTAV-Departamento de Nanociencia y Nanotecnología, Unidad Querétaro, 76230 Queretaro, Mexico

[∥]Departamento de Física Fundamental II, Instituto de Materiales y Nanotecnología, MALTA Consolider Team, Universidad de La Laguna, 38205 Tenerife, Spain

[⊥]Departamento de Física Aplicada-ICMUV, MALTA Consolider Team, Universidad de Valencia, Edificio de Investigación, C/Dr. Moliner 50, Burjassot, 46100 Valencia, Spain

[#]Institute of Applied Physics, Academy of Sciences of Moldova, 2028 Chisinau, Moldova

ABSTRACT: We report on Raman scattering measurements in mercury digallium selenide (HgGa₂Se₄) up to 25 GPa. We also performed, for the low-pressure defect-chalcopyrite structure, lattice-dynamics *ab initio* calculations at high pressures which agree with experiments. Measurements evidence that the semiconductor HgGa₂Se₄ exhibits a pressure-induced phase transition above 19 GPa to a previously undetected structure. This transition is followed by a transformation to a Raman-inactive phase above 23.4 GPa. On downstroke from 25 GPa until 2.5 GPa, a broad Raman spectrum was observed, which has been attributed to a fourth phase, and whose pressure dependence was followed during a second upstroke. Candidate structures for the three phases detected under compression are proposed. Finally, we also report and discuss the decomposition of the sample by laser heating at pressures close to 19 GPa. As possible products of decomposition, we have identified at least the formation of trigonal selenium nanoclusters and cinnabar-type HgSe.
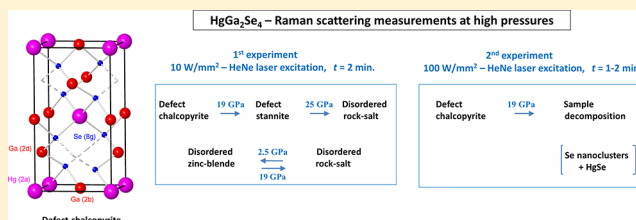
I. INTRODUCTION

Mercury digallium selenide (HgGa₂Se₄) is a semiconductor crystallizing in the tetragonal defect-chalcopyrite (DC) structure (space group (S.G.) $I\overline{4}$, No. 82, $Z = 2$).[1,2] It is one of the less studied adamantine-type $A^{II}B_2^{III}X_4^{VI}$ ordered-vacancy compounds (OVCs). Unlike binary zinc-blende-type AX materials,[3] OVCs are tetrahedrally coordinated ternary semiconductors derived from the cubic diamond or zinc-blende structure (S.G. $F\overline{4}3m$, No. 216, $Z = 4$) with vacancies located in an ordered and stoichiometric fashion at a fixed Wyckoff position in the unit cell due to the unbalanced number of anions and cations.

The presence of vacancies in the unit cell leads to a more complex physics in adamantine-type OVCs than in common semiconductors. A usual trend in OVCs is that they have several nonequivalent tetrahedrally coordinated cations resulting in a distortion of the crystal lattice from cubic symmetry. The symmetry reduction provides them special properties with important applications in optoelectronics, solar cells, and nonlinear optics.[3−6] Among the applications of $A^{II}B_2^{III}X_4^{VI}$ OVCs, we highlight their use as infrared-transmitting window materials and in various nonlinear optical devices, especially as gyrotropic media in narrow-band optical filters. In addition,

these compounds are promising optoelectronic materials due to their high values of nonlinear susceptibility, optical activity, intense luminescence, and high photosensitivity.[4] They are interesting in photovoltaic applications,[7] and as diluted magnetic semiconductors[8] as well. Furthermore, compounds like CdGa₂Se₄ and CdAl₂S₄ have practical applications as tunable filters and ultraviolet photodetectors.[9,10]

OVCs are also relevant materials in solid state physics from a theoretical point of view. They are useful to understand the role played by stoichiometric vacancies in the physical and chemical properties of solids. Note that OVCs constitute a bridge between perfect materials (with no vacancies at all) and defect materials (with random vacancies as point defects). Furthermore, OVCs are interesting for studying the order−disorder phase transitions occurring in tetrahedral semiconductors.

High-pressure (HP) studies on $A^{II}B_2^{III}X_4^{VI}$ compounds are receiving increasing interest.[11−35] In particular, the AGa₂Se₄ (A = Mn, Zn, and Cd) family has been recently studied by means of X-ray diffraction (XRD), Raman spectroscopy, and optical

absorption measurements. In the last years, we have conducted several studies of $HgGa_2Se_4$ at HP. Optical absorption and powder XRD under pressure in the defect chalcopyrite phase were studied in refs 28 and 32. On the other hand, recent powder HP XRD measurements in $HgGa_2Se_4$ have reported a transition from the ordered DC structure to the disordered rock-salt (DR) phase (S.G. $Fm\bar{3}m$, No. 225, $Z = 1$) on upstroke.[33] Furthermore, the transition to a disordered zinc-blende (DZ) phase (S.G. $F\bar{4}3m$, No. 216, $Z = 1$) on downstroke with recovery of the initial DC phase at 1.5 GPa after a thermal annealing was also reported.[33] These results are in good agreement with similar pressure-induced transitions in other selenium-based OVCs, like $CdGa_2Se_4$,[16] $MnGa_2Se_4$,[23] $CdAl_2Se_4$,[24] $ZnGa_2Se_4$,[25] and $HgAl_2Se_4$.[26]

To complement previous studies in $DC-HgGa_2Se_4$, we report here HP Raman scattering measurements up to 25 GPa. We also performed *ab initio* lattice-dynamics calculations to help in the assignment and discussion of the Raman-active modes of the DC phase. Above 19 GPa, Raman measurements suggest a phase transition from the DC structure, probably to a defect stannite (DS) structure (S.G. $I\bar{4}2m$, No. 121, $Z = 2$), that was not evidenced previously by XRD measurements.[32,33] A pressure-induced phase transition, prior to the phase transition to the Raman-inactive structure, was already proposed on the basis of Raman scattering results in $CdGa_2Se_4$[31] and evidenced by Raman scattering in $HgGa_2S_4$.[34] Furthermore, on decreasing pressure after the transition to the DR structure, a broad Raman spectrum, similar to those found in $CdGa_2Se_4$[31] and $ZnGa_2Se_4$[35] under similar conditions, was obtained. The broad Raman spectrum has been tentatively attributed to the metastable DZ phase already observed in ref 33 on downstroke. Raman spectra of this phase at HP were measured during a second pressure cycle. Finally, we also report results of a second experiment evidencing sample decomposition induced by laser heating at pressures close to the first transition pressure. The evolution of the Raman spectra with pressure during the second experiment allowed us to identify the presence of trigonal selenium, cinnabar-type HgSe, and likely Ga_2Se_3. Technical aspects of the experiments and calculations are given in sections II and III. The results are presented and discussed in section IV. Finally, we present the conclusions of this work in section V.

II. EXPERIMENTAL SECTION

Single crystals of $DC-HgGa_2Se_4$ were grown from its constituents HgSe and Ga_2Se_3 by the chemical vapor transport method using iodine as a transport agent.[36] The as-grown crystals represent triangular prisms with mirror surfaces. Chemical and structural analyses have shown the stoichiometric composition of the crystals, and no spurious phases were observed. The $DC-HgGa_2Se_4$ samples used in this study were the same used in three previous studies.[28,32,33] Evidence for the purity of our samples is provided by both XRD[32,33] and Raman scattering (here reported) measurements at ambient pressure which compare nicely with the available literature.

Nonresonant HP Raman scattering measurements at room temperature were performed with a LabRAM HR UV microspectrometer coupled to a Peltier-cooled CCD camera and using a 632.81 nm (1.96 eV) HeNe laser excitation line with a power of 10 mW and a spectral resolution better than 2 cm^{-1}. In order to analyze the Raman spectra under pressure, Raman peaks have been fitted when possible to a Voigt profile (Lorentzian profile convoluted by a Gaussian due to the limited resolution of the spectrometer) where the spectrometer

resolution is a fixed parameter. Otherwise, Raman peaks were fitted with Gaussians, where the spectrometer resolution was subtracted to get the real peak width. For Raman experiments, samples were loaded in a diamond-anvil cell (DAC) using a 16:3:1 methanol–ethanol–water mixture as a pressure-transmitting medium which exhibits reasonable quasi-hydrostatic behavior in the pressure range studied.[37] Ruby grains evenly distributed in the pressure chamber were used to measure the pressure by the ruby fluorescence method.[38,39] The shape and separation of the R_1 and R_2 ruby lines were checked at each pressure, and neither a significant increase in width nor an overlapping of both peaks were detected, thus suggesting that nearly quasi-hydrostatic conditions are fulfilled in our experiments.

We have performed two HP experiments of nonresonant Raman scattering. In the first one, fluxes of the order of 10 W/mm^2 and measurement times of around 2 min were used to avoid radiation damage to the sample by the incoming laser. To check the absence of heating effects, the sample was visually inspected before and after each measurement, and the Raman signal intensity was monitored during several accumulations in order to detect possible heating effects which could reduce the Raman signal or shift the Raman mode frequencies. In this experiment, Raman measurements were carried out until 25 GPa during the first upstroke and until almost ambient pressure during the first downstroke. Additionally, we measured Raman scattering up to 20 GPa during a subsequent second upstroke and down to ambient pressure during a second downstroke.

In the second experiment, we explored the effect of laser heating. We observed that performing Raman measurements with a higher power density (100 W/mm^2) of the incoming laser in similar conditions as those in the first experiment (measurement times of 1–2 min and several accumulations) can easily cause local damage in the sample. The damage occurred at HP near the pressure (19 GPa) where changes in the Raman spectrum are detected in the first experiment. In order to study the effect of laser heating in $HgGa_2Se_4$, we decreased the pressure until almost ambient pressure after realizing that new peaks appeared as a consequence of laser heating. Since the peaks remained on decreasing pressure, we performed HP Raman scattering measurements during a second upstroke in order to check the pressure dependence of the new Raman peaks.

III. THEORETICAL CALCULATION DETAILS

First principles total-energy and lattice-dynamics calculations were performed within the framework of the density functional theory (DFT) and the pseudopotential method using the Vienna *ab initio* simulation package (VASP) of which a detailed account can be found in ref 40. The exchange and correlation energy has been taken in the generalized gradient approximation (GGA) according to the Perdew–Burke–Ernzerhof (PBE) prescription.[41] Details of total-energy and lattice-dynamics calculations in the ordered DC structure for AGa_2Se_4 (A = Cd, Hg) can be consulted in refs 28 and 31. In this work, we only report calculations for the ordered DC structure at different pressures. We do not report calculations neither for the DZ phase nor for the DS phase of $HgGa_2Se_4$. Note that more than five different possible polytypes for the DS phase in OVCs have been previously suggested.[31,42−44] Furthermore, the DZ structure and several disordered DS polytypes have fractional atomic occupancies, thus requiring large supercells to simulate disorder using standard *ab initio*
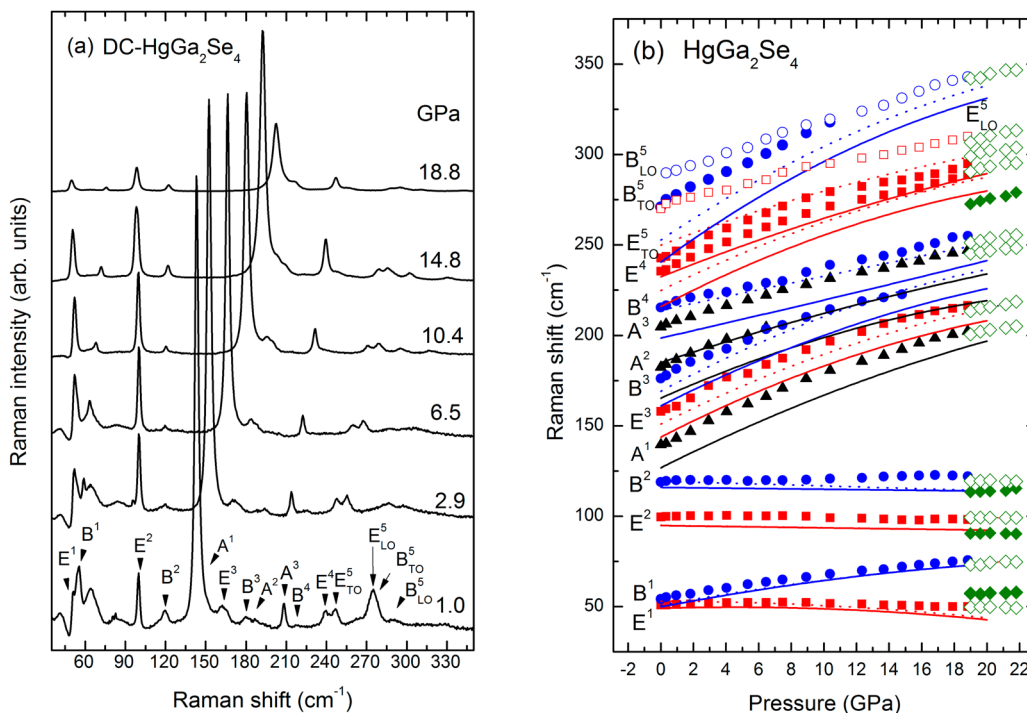
Figure 1. (a) Room-temperature Raman scattering spectra of DC-HgGa$_2$Se$_4$ up to 18.8 GPa. Arrows indicate the frequencies and symmetry of the Raman modes at 1.0 GPa. (b) Pressure dependence of the experimental (symbols) and calculated (lines) vibrational modes in HgGa$_2$Se$_4$ up to 22.4 GPa. Experimental values of A, B_{TO}/B_{LO}, and E_{TO}/E_{LO} Raman modes are represented by solid triangles (black), solid/open circles (blue), and solid/open squares (red), respectively. Theoretical calculations for the TO (LO) phonons of pure B and E symmetry are represented by solid (dotted) lines with blue and red colors, respectively. In the case of A modes, calculations are shown by solid black lines. The solid/open rhombuses (green) represent the modes of the new phase above 19 GPa.

methods. Such calculations become very time-consuming and the relaxed structure does not always maintain the original symmetry. This is what happened to our calculations for the DZ structure, whose supercell relaxed into a noncubic structure. Therefore, those calculations are not reported in this work.

Lattice dynamics calculations of phonon modes for the DC structure were performed at the zone center (Γ point) of the Brillouin zone. For the calculation of the dynamical matrix at Γ, we used the direct force-constant approach (or supercell method)[45,46] which involves the calculation of all the atomic forces when each non-symmetry-related atom in the unit cell is displaced along non-symmetry-related directions. Details of the lattice dynamics calculations in the DC structure can be consulted in ref 31.

In order to include the LO−TO splitting in our study, we need to add the effect of the electric field, which is not directly taken into account by the force-constant method. To obtain the LO−TO splitting with VASP, we have to add to the dynamical matrix a nonanalytical term, which depends on the Born effective charge tensors and the electronic dielectric constant. If an exact solution close to the Γ point is required, one needs to use different supercell sizes for each pressure, making this method very expensive in time. However, we checked that similar TO and LO phonon frequencies at the Γ point, but with lower CPU-time requirements, were found using density functional perturbation theory (DFPT)[47] with the Quantum Espresso package.[48] In this software, we added the nonanalytic term, due to the long-range interaction, using the response of the system to the electric field, which allows us to obtain the LO−TO splitting near the Γ point. Therefore, we can calculate the pure B and E modes with TO and LO splitting. In this

context, we used ultrasoft pseudopotentials with a cutoff energy of 60 Ry and a k-mesh of (4 4 4) in order to obtain well converged results. Moreover, the same exchange correlation energy prescription was used in the total energy and lattice dynamics DFPT calculations. Therefore, in the following, we will only present theoretical results for Raman-active modes of the DC phase including the LO−TO splitting obtained with the Quantum Espresso package.

IV. RESULTS AND DISCUSSION

A. First Experiment. According to group theory, DC-HgGa$_2$Se$_4$ has 15 vibrational modes[49]

$$\Gamma = 3A(R) + 6B(R, IR) + 6E(R, IR)$$

B and E modes are polar modes which are both Raman (R) and infrared (IR) active, while A modes are nonpolar modes which are only Raman active. All modes are noted hereafter with a superindex in order of increasing frequency. Both B modes and doubly degenerated E modes may exhibit longitudinal−transversal optic (LO−TO) splitting, and because of the crystal anisotropy, some modes could show mixed B and E symmetry.[50,51] Two of the 15 vibrational modes (an E mode and a B mode) are acoustic modes. Therefore, we expect 13 Raman-active optical modes: $3A + 5B + 5E$ and 10 IR-active optical modes: $5B + 5E$. Taking into account the LO−TO splitting, one could measure a maximum of 23 Raman-active first-order modes and 20 IR-active modes.

Figure 1a shows the Raman spectra at room temperature of DC-HgGa$_2$Se$_4$ up to 18.8 GPa during the first experiment. The Raman spectrum at low pressures is dominated by the A^1 mode attributed to the breathing mode of Se atoms around the

Table 1. Experimental and Theoretical Raman Mode Frequencies and Their Pressure Coefficients at Zero Pressure Derived from a Fit with $\omega(P) = \omega_0 + a_1 P + a_2 P^{2a}$

mode symmetry	$\omega_0{}^b$ (cm^{-1})	$a_1{}^b$ (cm^{-1} GPa^{-1})	$a_2 \times 100^b$ (cm^{-1} GPa^{-2})	$\omega_0{}^c$ (cm^{-1})	$a_1{}^c$ (cm^{-1} GPa^{-1})	$a_2 \times 100^c$ (cm^{-1} GPa^{-2})	$\omega_0{}^d$ (cm^{-1})
E^1_{TO}	51.1	0.30	−2.3	49.1	0.26	−2.9	51
E^1_{LO}				53.0	−0.02	−2.2	55
B^1_{TO}	54.7	1.50	−2.1	49.9	1.73	−2.7	
B^1_{LO}				50.9	1.60	−2.3	
E^2_{TO}	100.1	0.03	−0.8	94.9	−0.13		100
E^2_{LO}				95.0	−0.13		
B^2_{TO}	119.5	0.07	5.9	116.0	−0.10		121
B^2_{LO}				119.3	−0.26		
A^1	139.2	4.72	−7.3	126.8	4.53	−5.1	141
E^3_{TO}	157.8	4.66	−8.5	143.8	4.65	−7.2	162
E^3_{LO}				150.9	4.54	−6.7	
B^3_{TO}	176.4	4.72	−10.6	161.2	4.55	−6.6	186
B^3_{LO}				169.1	4.86	−7.4	
A^2	182.6	4.45	−18.0	165.4	4.00	−6.5	181
A^3	205.4	2.86	−3.6	185.0	2.97	−2.6	208
B^4_{TO}	216.3	2.01	0.4	198.6	2.04	0.5	218
B^4_{LO}				213.9	1.91	−0.2	
E^4_{TO}	235.8	4.17	−7.6	215.9	4.71	−7.5	237
E^4_{LO}				224.8	4.43	−6.4	
E^5_{TO}	242.8	4.47	−9.7	232.3	3.61	−3.7	245
E^5_{LO}	271.5	2.54	−2.85	249.9	3.48	−4.7	271
B^5_{TO}	272.3	4.90	−5.94	240.4	6.60	−10.3	245
B^5_{LO}	288.4	3.08	−0.92	252.7	6.07	−9.0	274

[a] Raman-active optical modes measured at ambient pressure[59] are also given for comparison. [b] Experimental Raman data (this work). [c] Theoretical calculations (this work). [d] Experimental Raman data (ref 59).

vacancies,[52] as it has been observed in other OVCs.[11,13,18,20−24,31,34] The Raman spectrum of DC-HgGa$_2$Se$_4$ can be divided into three regions: low-frequency region (below 130 cm^{-1}), medium-frequency region (between 130 and 200 cm^{-1}), and high-frequency region (above 200 cm^{-1}). As pressure increases, the Raman peaks of the medium- and high-frequency regions shift to higher frequencies, while most of the peaks of the low-frequency region show a negligible or even negative pressure coefficient. This behavior is similar to that found in other OVCs under pressure.[11,13,18,20−24,31,34]

Figure 1b shows the pressure dependence of the experimental and theoretical Raman mode frequencies of DC-HgGa$_2$Se$_4$ up to 18.4 GPa. In general, there is a rather good agreement between experimental and calculated Raman mode frequencies and their pressure coefficients at zero pressure, which are summarized in Table 1.

In order to understand the HP behavior of the Raman modes in OVCs, and in particular in HgGa$_2$Se$_4$, it is important to take into account that both tetragonal DS and DC structures derive from the zinc-blende structure by a doubling of the unit cell along the c axis. This results in a folding of the X and W points of the Brillouin zone edge of the zinc-blende structure into the Γ point of these two tetragonal structures. Therefore, several Raman modes in the tetragonal DC and DS structures behave similarly to vibrational modes occurring at the X and W points of the cubic zinc-blende structure. With this in mind, the very small or even negative pressure coefficients of the low-frequency E and B modes can be understood assuming that these two modes derive from transverse acoustic (TA) and longitudinal acoustic (LA) modes, respectively, at the X and W points of the Brillouin zone of the zinc-blende structure.[11,18,53,54] A similar HP effect was observed in chalcopyrites, like CuGaS$_2$.[55] On the basis of the comparison of the Raman

modes of DC and DS structures and those of the zinc-blende structure, it is possible to understand why the Raman modes of DS and DC structures located in the medium-frequency region exhibit the largest frequency pressure coefficients and why the modes of the high-frequency region exhibit a little bit smaller frequency pressure coefficients than the modes of the medium-frequency region. The explanation is that modes of the medium-frequency and high-frequency regions can be considered to be analogues of the TO and LO modes in the zinc-blende structure, where TO modes exhibit usually larger pressure coefficients than LO modes, a signature of the decrease of the ionicity of the semiconductor upon compression.[56−58]

In regard to the values of the measured Raman frequencies at ambient pressure, we must note that they correlate reasonably well with those previously reported in ref 59 (see Table 1), except for some differences. In particular, the lowest-frequency phonon B^1 that we have measured at 54.3 cm^{-1} seemingly was attributed to the E^1_{LO} mode in ref 59. Another difference is that in our measurements the B^3 mode has a lower frequency at ambient pressure than the A^2 mode while the opposite seems to be reported in ref 59. The last difference in Raman assignments between this work and ref 59 is the assignment for the highest-frequency modes. We have attributed the three modes of highest frequency to the E^5_{LO}, B^5_{TO}, and B^5_{LO} modes in order of increasing frequency, while in ref 59 the mode at 263 cm^{-1}, which we have attributed to the E^5_{LO} mode, was not observed and the last two were assigned as E^5_{LO} and B^5_{LO} modes. Our experimental and theoretical frequencies at ambient pressure can also be compared with the already reported experimental IR-active optical modes at ambient pressure.[60,61] In general, our experimental and theoretical values for polar E and B modes agree with those measured by IR reflectivity, except for the B^1

and B^2 modes. These two modes measured by IR reflectivity around 120 and 160 cm^{-1}, respectively, do not agree with our measured and calculated values, which are substantially smaller.

Above 18.8 GPa, we observed changes in the Raman spectrum of HgGa$_2$Se$_4$. Figure 2 shows the Raman spectrum of
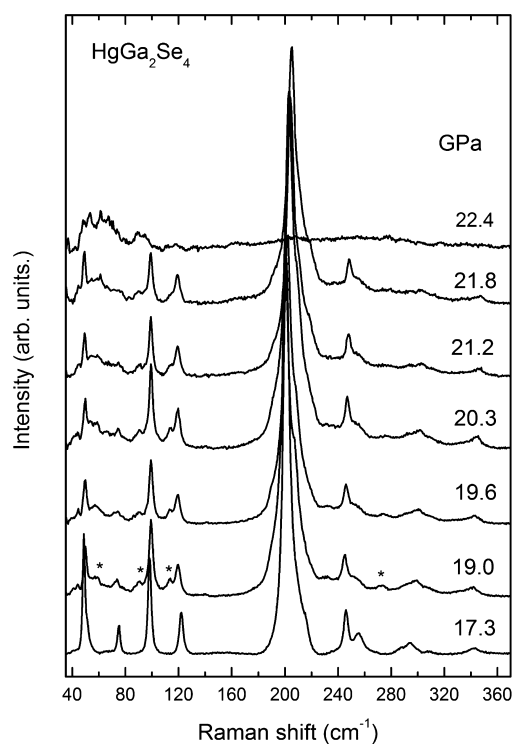

Figure 2. Room-temperature Raman scattering spectra of HgGa$_2$Se$_4$ at selected pressures. The Raman spectrum of the DC phase at 17.3 GPa is shown for comparison. Asterisks mark the new peaks of the new phase appearing above 19.0 GPa.

HgGa$_2$Se$_4$ at room temperature from 17.3 up to 22.4 GPa. Several extra Raman peaks are clearly observed (see asterisks) above 19 GPa, and most of the Raman peaks that seem to correspond to the original DC phase suffer a small shift in frequency. The frequencies of all modes observed above 19 GPa are shown in Figure 1b (see rhombuses). We will show that the observed changes suggest that a phase transition occurs above 19 GPa in HgGa$_2$Se$_4$ prior to the phase transition to the Raman-inactive DR phase occurring above 22.4 GPa. In this context, it is interesting to note that the pressure-driven transition from the completely ordered DC structure to the completely disordered rock-salt (DR) structure, observed by XRD measurements in OVCs,[16,23−26,33] was considered to be associated with a disorder increase,[11,13,24] as it occurs with temperature-induced transitions of many OVCs from the completely ordered DC structure to the completely disordered zinc-blende (DZ) structure.[62] We have shown in a previous study of a thermally activated cation ordering in ZnGa$_2$Se$_4$ crystal at ambient pressure the small differences in the Raman spectra of the DC phase and one of the polytypes of the DS phase.[63] However, in the literature, several polytypes of the DS phase with more Raman modes than the original DC phase have been proposed.[31,34,44] Therefore, on the basis of the extra Raman modes observed above 19 GPa and the shift of the modes previously attributed to the DC phase, we tentatively propose that HgGa$_2$Se$_4$ undergoes a DC-to-DS phase transition

above 19 GPa. This involves a partial cation-vacancy disorder and consequently an increase in the number of Raman modes likely due to the occupancy of 2b sites in the DS phase.[34] These sites were previously occupied by vacancies in the ordered DC phase, and thus, they did not contribute with any Raman mode in the DC phase.

In order to characterize the new phase tentatively assigned as DS, we increased the pressure from 18.8 GPa in small steps until the sample loses its Raman signal above 22.4 GPa, likely due to its transition to the DR phase observed in ref 33 and in good agreement with what was found in a number of defect chalcopyrites under pressure.[16,23−26,31,34] In this respect, we want to note that the detection of an intermediate phase between the DC and DR phases in HgGa$_2$Se$_4$ apparently contradicts the direct DC−DR transition detected by XRD experiments.[33] However, we think this apparent discrepancy can be caused by the laser absorption during Raman experiments, which may work as a thermal annealing, providing the thermal energy needed to induce the transition to the intermediate DS phase. Note that the DS phase is also observed in many OVCs at ambient pressure and moderate temperatures,[62] so it is probably not observed in XRD experiments due to the presence of kinetic barriers.[64,65] We want to stress here that in ref 33 the DC-to-DR phase transition in HgGa$_2$Se$_4$ was found to occur at 17 GPa, a pressure considerably lower than that reported by our Raman measurements. This was because MgO was used as a pressure transmitting medium in ref 33 and the non-hydrostatic conditions thus generated favor the occurrence of the phase transition at lower pressures.[66−68]

After the transition to the DR phase, we raised the pressure up to 25 GPa in order to complete the phase transition to the DR phase (as checked by the darkness and absence of a Raman signal in several regions of the sample). Afterward, we decreased the pressure slowly to 2.5 GPa and we found that the sample showed a new Raman spectrum below 5 GPa which did not correspond to the original DC phase nor to the intermediate phase found at 19 GPa in the first upstroke. The new Raman spectrum, shown in Figure 3, exhibits broad and overlapped bands. It looks like a one-phonon density of states typical of a completely disordered or amorphous structure. The broad bands of the new Raman spectrum can be compared to the relatively narrow Raman modes of the DC phase and the new phase reported in Figures 1a and 2. As it can be observed, the Raman spectrum on downstroke cannot be attributed to the Raman-inactive DR phase and cannot correspond to the DC phase nor the new phase shown in Figures 1a and 2. In this context, if we consider that the octahedrally coordinated DR phase is a totally disordered phase, we tentatively attribute the Raman spectrum on downstroke to the DZ phase (detected in XRD experiments[33]), which is a totally disordered tetrahedrally coordinated phase. Therefore, no order was recovered on decreasing pressure. The observation of the DZ phase on downstroke was previously found in several HP XRD studies in OVCs.[16,24,26] Furthermore, we must note that similar assignments of broad Raman spectra to the DZ phase on decreasing pressure from the DR structure have been recently done in CdGa$_2$Se$_4$ and HgGa$_2$S$_4$.[31,34]

In order to study the Raman spectrum of the DZ phase, we performed Raman scattering measurements of the recovered sample during a second upstroke until 20 GPa. The Raman intensity strongly decreases beyond 14 GPa (see Figure 3). Finally, it must be stressed that our Raman scattering
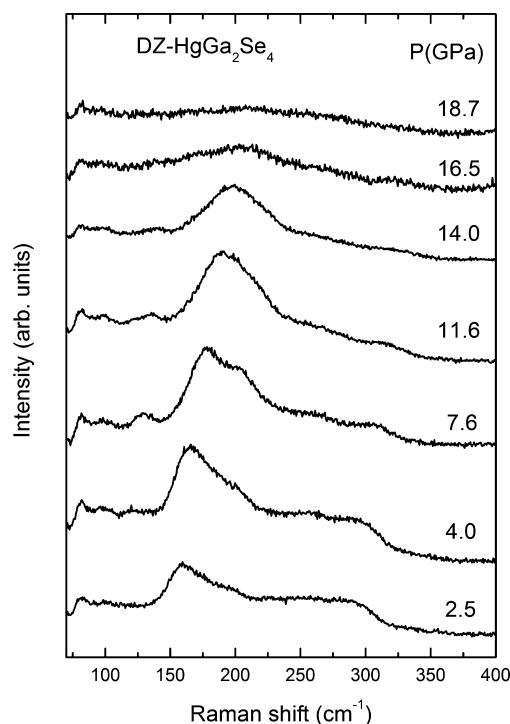
Figure 3. Room-temperature Raman scattering spectra of DZ-HgGa$_2$Se$_4$ up to 18.7 GPa.

Figure 4. Room-temperature Raman scattering spectra of HgGa$_2$Se$_4$ at selected pressures from 15.9 to 22.4 GPa corresponding to the first upstroke of the second experiment. The asterisk in the spectrum at 19.7 GPa marks a new broad band formed when the sample was damaged by the incoming laser radiation.

measurements under pressure suggest a reversible transition from the DZ to the DR phase above 19 GPa in HgGa$_2$Se$_4$.

In summary, the sequence of pressure-induced phase transitions observed in HgGa$_2$Se$_4$ (DC-DS-DR on upstroke and DR-DZ on downstroke) evidence the existence of an intermediate phase with partial cation-vacancy disorder between the ordered DC and the DR phases. They also evidence the irreversibility of the order−disorder DC-to-DR phase transition and the reversibility of the DZ-to-DR phase transition, in good agreement with previous high-pressure measurements in CdGa$_2$Se$_4$, HgGa$_2$S$_4$, and ZnGa$_2$Se$_4$.[31,34,35]

B. Second Experiment. Since apparently laser absorption influences the observed structural sequence in HgGa$_2$Se$_4$, we carried out a second experiment in order to study the effect of laser heating on the samples at HP. The first fact we noticed in these experiments was that the sample was locally damaged by the excessive laser excitation at pressures above 19 GPa, i.e., close to the transition to the intermediate phase between DC and DR structures. We think that the damage was caused by heating due to the local absorption of the laser energy due to the decrease of the absorption edge energy at the DC-to-DS phase transition but also likely due to the presence of some dark linear defects that appear in the sample as onset of the transition to the Raman−inactive phase[69] also noted in previous works in OVCs.[28,31,34] The temperature of the sample induced during laser absorption cannot be measured, but it can be estimated to be only a few hundred degrees, since no thermal emission was detected from the sample.[70]

Figure 4 shows the Raman spectrum of HgGa$_2$Se$_4$ at room temperature from 15.9 up to 22.4 GPa in a local zone damaged by the excessive laser power. New features appear in the Raman spectrum above 19.7 GPa due to laser heating (see asterisk in Figure 4). Note that during the first experiment the spectrum at 22.4 GPa was totally different from the one observed at the same pressure in the second experiment. We checked the
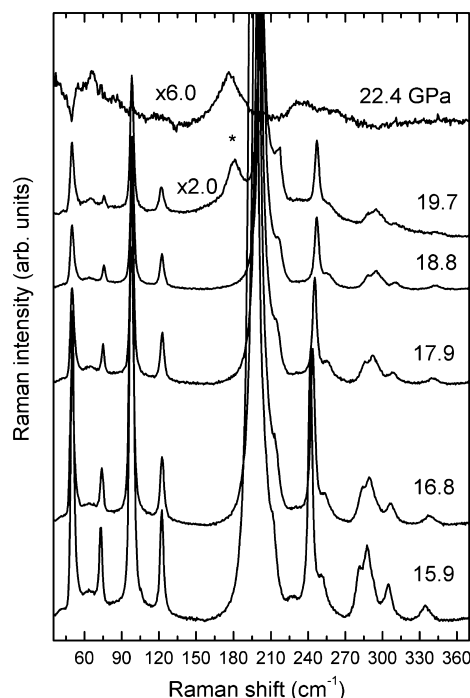
reproducibility of the Raman spectra in the damaged sample because similar spectra were observed in different damaged zones along the sample.

In order to check the reversibility of the observed changes due to laser heating, we decreased the pressure close to ambient pressure. Figure 5a shows the Raman spectrum at 2.2 GPa on decreasing pressure. Clearly, the Raman spectrum is completely different from those attributed to the DC phase, the new phase, and DZ phases during the first experiment and commented in the previous section. In the following, we will show that the new Raman modes correspond to the decomposition of the sample, which leads to the observation of Raman scattering of trigonal Se, cinnabar-type HgSe, and likely Ga$_2$Se$_3$. Curiously, laser-induced decomposition of ZnSe near the zinc-blende to rock-salt phase transition with the corresponding observation of Se nanoclusters has been recently reported.[71]

In order to investigate the nature of the species involved in the Raman signal after laser heating at HP, we performed Raman scattering measurements during a second upstroke to get information about the pressure dependence of the new Raman modes. Figure 5a shows the Raman scattering spectra at selected pressures until 24.3 GPa measured in a zone of the sample that was damaged by the incoming laser excitation. The different Raman modes observed are referred to by vertical arrows with numbers. Note that we have not taken into account Raman modes below 100 cm^{-1} because we are not confident about the behavior of those modes, which can be influenced by the steep edge caused by the edge filter of our single stage spectrometer. The pressure dependence of the frequencies of the six experimental Raman modes analyzed is shown in Figure 5b. We have identified four (bands 2, 3, 4, and 5) of the six Raman modes that correspond to the trigonal Se phase. This hypothesis is confirmed by the pressure dependence of these
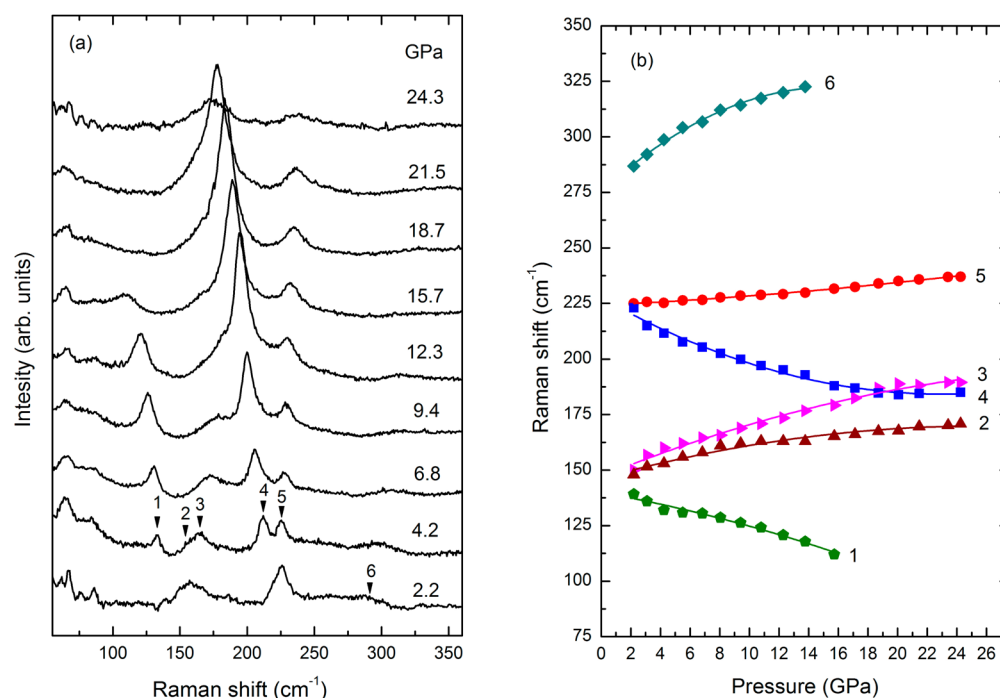
15778

dx.doi.org/10.1021/jp402493r | J. Phys. Chem. C 2013, 117, 15773−15781

Figure 5. (a) Room-temperature Raman scattering spectra of $HgGa_2Se_4$ at selected pressures up to 24.3 GPa corresponding to the second upstroke of the second experiment. Vertical arrows with numbers refer to the different Raman modes observed due to the damage of the sample caused by laser heating. (b) Pressure dependence of the experimental Raman mode frequencies observed in the second upstroke of the second experiment.

four modes which is similar to that of the Raman modes of the trigonal Se phase previously reported.[71−76] Among the four modes, the most distinct assignment is that of peak 4, which is characterized by a huge negative pressure coefficient and it has been associated with the trigonal Se A^1 mode.[71−76] On the other hand, a broad band around 280 cm^{-1} (number 6) that disappears above 14 GPa does not fit with the Raman modes of the known polytypes (ε, γ, δ) of GaSe[77] and could be tentatively ascribed to either α- or β-Ga_2Se_3, whose HP behavior was already partially reported and shows phase transitions to the Raman-inactive rock-salt phase around 14 GPa.[78−80]

Finally, as regards mode 1, it has a negative pressure coefficient (−2.0 cm^{-1}/GPa) and it seems to not be related to trigonal Se or Ga_2Se_3, since it disappears above 16 GPa. Furthermore, these compounds do not show a mode with negative pressure coefficient in the 130 cm^{-1} region. Mode 1 cannot correspond to α-HgSe with zinc-blende structure, since this phase, despite having a TO mode near 130 cm^{-1},[81] is stable only below 1.5 GPa and we decreased the pressure only until 2.2 GPa. Instead, we think that mode 1 could correspond to cinnabar-type HgSe, since this phase is stable between 1.5 and 16 GPa when a phase transition to the Raman-inactive rock-salt phase occurs.[82] Unfortunately, no Raman measurements have been reported for HgSe under pressure neither in the zinc blende nor in the cinnabar phase to our knowledge. However, Raman scattering measurements in cinnabar-type HgS under pressure report an intense mode above 200 cm^{-1} with a strong negative pressure coefficient.[83] In order to verify the attribution of the mode at 130 cm^{-1} to cinnabar-type HgSe, we have performed Raman scattering measurements and *ab initio* calculations at different pressures for cinnabar-type HgSe (to be reported elsewhere) and we have found a Raman-active A_1 mode near 130 cm^{-1} with a negative pressure coefficient similar to that of mode 1 in Figure 5. In fact, previous theoretical

results suggested the presence of a phonon around 130 cm^{-1} which softens with pressure;[84] however, these authors do not report either the mode symmetry or the pressure coefficient. Therefore, we can safely attribute mode 1 with negative pressure coefficient to cinnabar-type HgSe. Its frequency, pressure coefficient, and observation between 2 and 16 GPa are in good agreement with our Raman measurements and *ab initio* calculations for the A_1 mode of cinnabar-type HgSe and with previous XRD measurements that show the phase transition from the cinnabar to the Raman-inactive rock-salt structure above 16 GPa.

In summary, our Raman measurements with high laser power provide evidence of the local decomposition of the $HgGa_2Se_4$ sample near 19 GPa. Local decomposition by laser heating due to absorption of the laser energy occurs near the focus of the laser spot and leads to the formation of Se nanoclusters, HgSe, and likely Ga_2Se_3.

V. CONCLUSIONS

We have performed Raman scattering measurements in DC-$HgGa_2Se_4$ under high pressure. Our measurements and calculations provide evidence that the ordered defect chalcopyrite phase undergoes a progressive cation-vacancy disorder on increasing pressure that results in a phase transition toward a new phase that could be attributed to the partially disordered defect stannite phase, which is prior to the phase transition to the disordered rock-salt structure. The transition to the intermediate partially disordered structure was not detected in prior XRD experiments in $HgGa_2Se_4$, so we cannot discard that it could be enhanced by thermal annealing caused by laser absorption. We have also observed that, once the transition to the Raman-inactive phase is completed near 25 GPa, a different metastable disordered phase is formed on decreasing pressure below 5 GPa. Therefore, the tentative sequence of phase transitions reported for $HgGa_2Se_4$ (DC →

15779

dx.doi.org/10.1021/jp402493r | J. Phys. Chem. C 2013, 117, 15773−15781

DS → DR) on upstroke suggests the existence of an intermediate phase with partial cation-vacancy disorder between the ordered defect chalcopyrite phase and the disordered rock-salt phase, as already proved in HgGa$_2$S$_4$.[34] On the other hand, the sequence of phase transitions and DR → DZ on downstroke and DZ → DR on upstroke evidence the irreversibility of the pressure-induced order−disorder processes and the reversibility of disorder−disorder processes occurring in this ordered-vacancy compound.

A second experiment, where laser-heating-induced damage was caused to the sample at high pressures, has shown the decomposition of the sample. After decreasing pressure near 2 GPa, on recompression, the presence of trigonal Se, cinnabar-type HgSe, and likely Ga$_2$Se$_3$ were identified by the pressure dependence of the observed Raman modes. Therefore, this experiment stresses the importance of controlling laser excitation in HgGa$_2$Se$_4$ and in other ternary chalcogenides in order to avoid local heating effects that could cause the decomposition of the samples as it has been observed in binary chalcogenides.[71]

■ AUTHOR INFORMATION

Corresponding Author
*E-mail: rovilap@fis.upv.es.

Notes
The authors declare no competing financial interest.

■ ACKNOWLEDGMENTS

■ REFERENCES

(1) Hahn, H.; Frank, G.; Klingler, W.; Stoerger, A. D.; Stoerger, G. Z. Anorg. Allg. Chem. **1955**, 279, 241.

(2) Gastaldi, L.; Simeone, M. G.; Viticoli, S. Solid State Commun. **1985**, 55, 605.

(3) MacKinnon, A. In Tables of Numerical Data and Functional Relationships in Science and Technology; Madelung, O., Schulz, M., Weiss, H., Eds.; Landolt-Börnstein New Series, Group III, Vol. 17, pt. h; Springer-Verlag: Berlin, 1985; p 124.

(4) Georgobiani, A. N.; Radautsan, S. I.; Tiginyanu, I. M. Sov. Phys. Semicond. **1985**, 19, 121.

(5) Bernard, J. E.; Zunger, A. Phys. Rev. B **1988**, 37, 6835.

(6) Jiang, X.; Lambrecht, W. R. L. Phys. Rev. B **2004**, 69, 035201.

(7) Zunger, A.; Wagner, S.; Petroff, P. M. J. Electron. Mater. **1993**, 22, 3.

(8) Millan, A.; Moron, M. C. J. Appl. Phys. **2001**, 89, 1687.

(9) Radautsan, S. I.; Tiginyanu, I. M. Jpn. J. Appl. Phys. **1993**, 32S3, 5.

(10) Joshi, N. V.; Luengo, J.; Vera, F. Mater. Lett. **2007**, 61, 1926.

(11) Burlakov, I. I.; Raptis, Y.; Ursaki, V. V.; Anastassakis, E.; Tiginyanu, I. M. Solid State Commun. **1997**, 101, 377.

(12) González, J.; Rico, R.; Calderón, E.; Quintero, M.; Morocoima, M. Phys. Status Solidi B **1999**, 211, 45.

(13) Ursaki, V. V.; Burlakov, I. I.; Tiginyanu, I. M.; Raptis, Y. S.; Anastassakis, E.; Anedda, A. Phys. Rev. B **1999**, 59, 257.

(14) Fuentes-Cabrera, M.; Sankey, O. F. J. Phys.: Condens. Matter **2001**, 13, 1669.

(15) Fuentes-Cabrera, M. J. Phys.: Condens. Matter **2001**, 13, 10117.

(16) Grzechnik, A.; Ursaki, V. V.; Syassen, K.; Loa, I.; Tiginyanu, I. M.; Handfland, M. J. Solid State Chem. **2001**, 160, 205.

(17) Takumi, M.; Ueda, T.; Koshio, Y.; Nishimura, H.; Nagata, K. Phys. Status Solidi B **2001**, 223, 271.

(18) Mitani, T.; Onari, S.; Allakhverdiev, K.; Gashimzade, F.; Kerimova, T. Phys. Status Solidi B **2001**, 223, 287.

(19) Tatsi, A.; Lampakis, D.; Liarokapis, E.; López, S. A.; Martínez, L.; Giriat, W. High Pressure Res. **2002**, 22, 89.

(20) Tiginyanu, I. M.; Ursaki, V. V.; Manjón, F. J.; Tezlevan, V. E. J. Phys. Chem. Solids **2003**, 64, 1603.

(21) Mitani, T.; Naitou, T.; Matsuishi, K.; Onari, S.; Allakhverdiev, K.; Gashimzade, F.; Kerimova, T. Phys. Status Solidi B **2003**, 235, 321.

(22) Allakhverdiev, K.; Gashimzade, F.; Kerimova, T.; Mitani, T.; Naitou, T.; Matsuishi, K.; Onari, S. J. Phys. Chem. Solids **2003**, 64, 1597.

(23) Marquina, J.; Power, Ch.; Grima, P.; Morocoima, M.; Quintero, M.; Couzinet, B.; Chervin, J. C.; Munsch, P.; González, J. J. Appl. Phys. **2006**, 100, 093513.

(24) Meenakshi, S.; Vijyakumar, V.; Godwal, B. K.; Eifler, A.; Orgzall, I.; Tkachev, S.; Hochheimer, H. D. J. Phys. Chem. Solids **2006**, 67, 1660.

(25) Errandonea, D.; Kumar, R. S.; Manjón, F. J.; Ursaki, V. V.; Tiginyanu, I. M. J. Appl. Phys. **2008**, 104, 063524.

(26) Meenakshi, S.; Vijyakumar, V.; Eifler, A.; Hochheimer, H. D. J. Phys. Chem. Solids **2010**, 71, 832.

(27) Singh, P.; Sharma, M.; Verma, U. P.; Jensen, P. Z. Kristallogr. **2010**, 225, 508.

(28) Manjón, F. J.; Gomis, O.; Rodríguez-Hernández, P.; Pérez-González, E.; Muñoz, A.; Errandonea, D.; Ruiz-Fuertes, J.; Segura, A.; Fuentes-Cabrera, M.; Tiginyanu, I.; Ursaki, V. V. Phys. Rev. B **2010**, 81, 195201.

(29) Jiang, X.-S.; Yan, Y.-C.; Yuan, S.-M.; Mi, S.; Niu, Z.-G.; Liang, J.-Q. Chin. Phys. B **2010**, 19, 10174.

(30) Meenakshi, S. J. Phys.: Conf. Ser. **2012**, 377, 012024.

(31) Gomis, O.; Vilaplana, R.; Manjón, F. J.; Pérez-González, E.; López-Solano, J.; Rodríguez-Hernández, P.; Muñoz, A.; Errandonea, D.; Ruiz-Fuertes, J.; Segura, A.; Santamaría-Pérez, D.; Tiginyanu, I. M.; Ursaki, V. V. J. Appl. Phys. **2012**, 111, 013518.

(32) Gomis, O.; Vilaplana, R.; Manjón, F. J.; Santamaría-Pérez, D.; Errandonea, D.; Pérez-González, E.; López-Solano, J.; Rodríguez-Hernández, P.; Muñoz, A.; Tiginyanu, I. M.; Ursaki, V. V. J. Appl. Phys. **2013**, 113, 073510.

(33) Gomis, O.; Vilaplana, R.; Manjón, F. J.; Santamaría-Pérez, D.; Errandonea, D.; Pérez-González, E.; López-Solano, J.; Rodríguez-Hernández, P.; Muñoz, A.; Tiginyanu, I. M.; Ursaki, V. V. Mater. Res. Bull. **2013**, 48, 2128.

(34) Vilaplana, R.; Robledillo, M.; Gomis, O.; Sans, J. A.; Manjón, F. J.; Pérez-González, E.; Rodríguez-Hernández, P.; Muñoz, A.; Tiginyanu, I. M.; Ursaki, V. V. J. Appl. Phys. **2013**, 113, 093512.

(35) Vilaplana, R.; Gomis, O.; Pérez-González, E.; Ortiz, H. M.; Manjón, F. J.; Rodríguez-Hernández, P.; Muñoz, A.; Tiginyanu, I. M.; Ursaki, V. V. High-pressure Raman scattering study of defect chalcopyrite and defect stannite ZnGa$_2$Se$_4$, just accepted to be published in. J. Appl. Phys. **2013**, 113, 233501.

(36) Tiginyanu, I. M.; Modovyan, N. A.; Stoika, O. D. Fiz. Tverd. Tela **1992**, 34, 967; Sov. Phys. Solid State **1992**, 43, 527.

(37) Klotz, S.; Chervin, J.-C.; Munsch, P.; Le Marchand, G. J. Phys. D: Appl. Phys. **2009**, 42, 075413.

(38) Mao, H. K.; Xu, J.; Bell, P. M. J. Geophys. Res. **1986**, 91, 4673.

(39) Syassen, K. High Pressure Res. **2008**, 28, 75.

(40) Kresse, G.; Hafner, J. Phys. Rev. B **1993**, 47, 558. Kresse, G.; Hafner, J. Phys. Rev. B **1994**, 49, 14251. Kresse, G.; Furthmüller, J. Comput. Mater. Sci. **1996**, 6, 15. Kresse, G.; Furthmüller, J. Phys. Rev. B **1996**, 54, 11169.

(41) Perdew, J. P.; Burke, K.; Ernzerhof, M. Phys. Rev. Lett. **1997**, 78, 1396.

(42) Eifler, A.; Hecht, J.-D.; Lippold, G.; Riede, V.; Grill, W.; Krauss, G.; Krämer, V. Physica B **1999**, 263−264, 806.

(43) Eifler, A.; Krauss, G.; Riede, V.; Krämer, V.; Grill, W. *J. Phys. Chem. Solids* **2005**, *66*, 2052.

(44) Manjón, F. J.; Gomis, O.; Vilaplana, R.; Sans, J. A.; Ortiz, H. M. *Phys. Status Solidi B* **2013**, DOI: 10.1002/pssb.201248596.

(45) Kreese, G.; Furthmüller, J.; Hafner, J. *Europhys. Lett.* **1995**, *32*, 729.

(46) Parlinski, K. *computer code PHONON*. See: http://www.computingformaterials.com/index.html.

(47) Baroni, S.; Gironcoli, S.; del Corso, A.; Giannozzi, P. *Rev. Mod. Phys.* **2001**, *73*, 515.

(48) Giannozzi, P.; Baroni, S.; Bonini, P.; et al. *J. Phys.: Condens. Matter* **2009**, *21*, 395502.

(49) Kroumova, E.; Arroyo, M. I.; Pérez-Mato, J. M.; Kirov, A.; Capillas, C.; Ivantchev, S.; Wondratschek, H. *Phase Transit.* **2003**, *76*, 155; Bilbao Crystallographic Server, http://www.cryst.ehu.es.

(50) Loudon, R. *Adv. Phys.* **1964**, *13*, 423.

(51) Alonso-Gutiérrez, P.; Sanjuán, M. L. *Phys. Rev. B* **2008**, *78*, 045212.

(52) Miller, A.; MacKinnon, A. K.; Weaire, D. *Solid State Phys.* **1981**, *36*, 119.

(53) Talwar, D. N.; Vandevyver, M.; Kunc, K.; Zigone, M. *Phys. Rev. B* **1981**, *24*, 741.

(54) Klotz, S.; Besson, J. M.; Braden, M.; Karch, K.; Pavone, P.; Strauch, D.; Marshall, W. G. *Phys. Rev. Lett.* **1997**, *79*, 1313.

(55) González, J.; Fernández, B. J.; Besson, J. M.; Polian, A. *Phys. Rev. B* **1992**, *46*, 15092.

(56) Sanjurjo, J. A.; López-Cruz, E.; Vogl, P.; Cardona, M. *Phys. Rev. B* **1983**, *28*, 4579 and references therein.

(57) Cardona, M. *J. Phys. C* **1984**, *8*, 29.

(58) Anastasakis, E.; Cardona, M. *High Pressure in Semiconductor Physics*; Academic: New York, 1998; Vol. 2, p 152 and references therein.

(59) Razzetti, C.; Lottici, P. P. *Jpn. J. Appl. Phys.* **1993**, *32*, 431.

(60) Hauseler, H.; Wäschenbach, G.; Lutz, H. D. *Phys. Status Solidi B* **1985**, *129*, 549.

(61) Hauseler, H. *J. Solid State Chem.* **1978**, *26*, 367.

(62) Garbato, L.; Ledda, F.; Rucci, A. *Prog. Cryst. Growth Charact.* **1987**, *15*, 1 and references therein.

(63) Vilaplana, R.; Gomis, O.; Pérez-González, E.; Ortiz, H. M.; Manjón, F. J.; Rodríguez-Hernández, P.; Munóz, A.; Alonso-Gutierrez, P.; Sanjuán, M. L.; Ursaki, V. V.; Tiginyanu, I. M. *J. Phys.: Condens. Matter* **2013**, *25*, 165802.

(64) Garcia-Domene, B.; Ortiz, H. M.; Gomis, O.; Sans, J. A.; Manjón, F. J.; Muñoz, A.; Rodríguez-Hernández, P.; Achary, S. N.; Errandonea, D.; Martínez-García, D.; Romero, A. H.; Singhal, A.; Tyagi, A. K. *J. Appl. Phys.* **2012**, *112*, 123511.

(65) Errandonea, D.; Somayazulu, M.; Häusermann, D. *Phys. Status Solidi B* **2002**, *231*, R1.

(66) Ruiz-Fuertes, J.; Errandonea, D.; Lacomba-Perales, R.; Segura, A.; González, J.; Rodríguez, F.; Manjón, F. J.; Ray, S.; Rodríguez-Hernández, P.; Muñoz, A.; Zhu, Zh.; Tu, C. Y. *Phys. Rev. B* **2010**, *81*, 224115.

(67) Gomis, O.; Sans, J. A.; Lacomba-Perales, R.; Errandonea, D.; Meng, Y.; Chervin, J. C.; Polian, A. *Phys. Rev. B* **2012**, *86*, 054121.

(68) Santamaría-Pérez, D.; Gracia, L.; Garbarino, G.; Beltrán, A.; Chulia-Jordan, R.; Gomis, O.; Errandonea, D.; Ferrer-Roca, Ch.; Martínez-García, D.; Segura, A. *Phys. Rev. B* **2011**, *84*, 054102.

(69) Manjón, F. J.; Errandonea, D.; Segura, A.; Chervin, J. C.; Muñoz, V. *High Pressure Res.* **2002**, *22*, 261.

(70) Errandonea, D. *J. Phys. Chem. Solids* **2006**, *67*, 2017.

(71) Lindberg, G. P.; Tallman, R. E.; Lauck, R.; Cardona, M.; Liu, X.; Furdyna, J. K.; Weinstein, B. A. *Phys. Status Solidi B* 250 No. 4, 711−715.

(72) Richter, W.; Renucci, J. B.; Cardona, M. *Phys. Status Solidi B* **1973**, *56*, 223.

(73) Aoki, K.; Shimomura, O.; Minomura, S.; Koshizuka, N.; Tsushima, T. *J. Phys. Soc. Jpn.* **1980**, *48*, 906.

(74) Bandyopadhyay, A. K.; Ming, L. C. *Phys. Rev. B* **1996**, *54*, 12049.

(75) Liu, H. Z.; Jin, C. Q.; Zhao, Y. H. *Physica B* **2002**, *315*, 210.

(76) Degtyareva, O.; Hernández, E. R.; Serrano, J.; Somayazulu, M.; Mao, H. K.; Gregoryanz, E.; Hemley, R. J. *J. Chem. Phys.* **2007**, *126*, 084503.

(77) Gauthier, M.; Poliann, A.; Besson, J. M.; Chevy, A. *Phys. Rev. B* **1989**, *40*, 3837.

(78) Finkman, E.; Tauc, J.; Kershaw, R.; Wold, A. *Phys. Rev. B* **1975**, *11*, 3785.

(79) Takumi, M.; Koshio, Y.; Nagata, K. *Phys. Status Solidi B* **1999**, *211*, 123.

(80) Takumi, M.; Hirata, A.; Ueda, T.; Koshio, Y.; Nishimura, H.; Nagata, K. *Phys. Status Solidi B* **2001**, *223*, 423.

(81) Szuszkiewicz, W.; Dynowska, E.; Gorecka, J.; Witkowska, B.; Jouanne, M.; Morhange, J. F.; Julien, C.; Hennion, B. *Phys. Status Solidi B* **1999**, *215*, 93.

(82) Huang, T.; Ruoff, A. L. *Phys. Rev. B* **1983**, *27*, 7811 and references therein.

(83) Werner, A.; Hochheimer, H. D.; Strössner, K.; Jayaraman, A. *Phys. Rev. B* **1983**, *28*, 3330.

(84) Radescu, S.; Mujica, A.; López-Solano, J.; Needs, R. J. *Phys. Rev. B* **2011**, *83*, 094107.